Proceedings of the ASME 2022 Conference on Smart Materials,
Adaptive Structures and Intelligent Systems
SMASIS2022
September 12-14, 2022, Dearborn, MI

SMASIS2022-91069

FLEXIBLE PIEZOELECTRIC WAVE-BASED SENSOR: NUMERICAL ANALYSIS AND VALIDATION

Rishikesh Srinivasaraghavan Govindarajan, Foram Madiyar, Daewon Kim
Embry-Riddle Aeronautical University, Daytona Beach, FL

ABSTRACT

The demand for acoustic wave-based devices has been rapidly increasing in the aerospace, chemical, and biological fields due to their versatility towards sensing measurands. This paper explores the characteristics and effectiveness of acoustic wave-based two-port sensors designed with bidirectional IDT electrodes placed in different configurations, such as surface mounted or embedded inside the substrate, through numerical and experimental analysis. The numerical study involves 3D modeling of the sensor design to investigate wave characteristics by utilizing time-domain, i.e., time delay and wave patterns, and frequency-domain analysis, i.e., scattering parameter study. The sensor made of polyvinylidene fluoride polymer is modeled to ensure the concordance between the theoretical and numerical results as well as a preliminary experimental result obtained from transparent piezoelectric films. The coupling of modes theoretical model is used to obtain the device's frequency response by a transmission matrix cascading technique. These investigated results will stand as guidance and facilitate defining an approach that can predict the behavior of the sensor with a specific design under different operating environments and expand its viability towards multi-functional devices that are reliable and sensitive to intended measurands.

Keywords: Piezoelectric, Acoustic sensor, COM, Numerical

1. INTRODUCTION

Piezoelectric wave-based sensors have gained increasing attention in a wide range of applications due to their advantages, such as small size, passive nature, fast response to environmental changes, and high sensitivity towards external parameters. Additionally, flexible structures and wearable technologies are evolving in recent days, particularly in the aerospace and biomedical sectors [1-4]. The necessity to monitor the deformations occurring in the structures demands a flexible sensor device to ensure safety. Modeling and optimization play a pivotal role in developing susceptible and portable devices before production by offering a substantial benefit in reducing time and money. Compared to other commercial sensors, piezoelectric wave-based sensors are highly sensitive with a stable fundamental frequency at higher frequency ranges and in harsh environments. These wave-based sensors mainly consist of a piezoelectric substrate, transmitting and receiving interdigital transducer (IDT) electrodes separated by a delay line. The voltage potential is provided to the input electrodes, where an alternative polarity with an electric field creation ends up in the form of a mechanical wave by utilizing piezoelectric effects. Constitutive equation [5] for the measurement of strain or electric displacement in the piezoelectric material is described in a quantitative form as,

$$S_p = s_{pq}^E T_q + d_{kp} E_k \quad (1)$$

$$D_i = d_{iq} T_q + \varepsilon_{jk}^S E_k \quad (2)$$

where S_p and T_q (Pa) describe the mechanical strain and stress components for the mechanical domain; D_i (Coulomb/m^2) and E_k (Volt/m) represent the electric charge density displacement and electric field for the electric domain; s_{pq}^E (Pa^{-1}), d_{kp} (Coulomb/N) and ε_{ik}^S denote the elastic stiffness, piezoelectric strain, and dielectric constants respectively. These equations are solved together with Maxwell's equation and the mechanical equations of motion to obtain a solution for the piezoelectric problem. Mainly, IDT design in the piezoelectric sensor is crucial, as the coupling between the electrode and piezoelectric substrate dictates the effectiveness of the wave propagation, providing useful information for desired parameters. However, a better interpretation of wave characteristics and design methodology has not yet been examined to understand the underlying multiphysics [6,7]. Generally, the IDT design is patterned through traditional techniques, such as photolithography and electron beam lithography [8], with a major cleanroom requirement limiting the mass production and complex lithographic photomask that can be averted by utilizing advanced two-photon polymerization (2PP) process [9,10]. The selected 2PP process allows extremely high-resolution parts in micro- and nano- scales that can be employed to sputter coat the pattern onto the substrate easily. Selecting a suitable piezoelectric substrate material is important in sensor development. Due to the lack of flexibility in other commonly used ceramics and single crystals [11], a semicrystalline polyvinylidene fluoride (PVDF) polymer

is selected as it exhibits piezoelectric properties with lightweight nature, mechanical compliance, and ease in processing. In this work, the wave-based piezoelectric sensor made of PVDF with different electrode configurations, such as surface mounted or embedded inside the substrate, is examined to study the sensor's generated wave characteristics and effectiveness through numerical, theoretical, and experimental analysis. Compared to the IDT electrodes deposited on the surface, studies demonstrate an enhancement of electrocoupling coefficient (k^2) [12] by embedding the electrodes to the substrate, where the IDTs will be protected from external damage with effective wave generation, expanding the range of applications to have a completely embedded sensor in the desired structures.

2. NUMERICAL AND THEORETICAL MODELING

The primary goal of the acoustic sensor is to be highly sensitive with low loss to the strain concentrations that occur in aerospace structures. To validate the sensor's performance with different electrode configurations, the wave-characteristics are examined using a numerical tool in the time-domain (voltage response and wave patterns) and frequency-domain (scattering parameter). The obtained frequency response is then validated using the theoretical model.

2.1 Numerical study

Computer-aided simulation, such as finite element method (FEM), helps efficiently design the piezoelectric sensor to study the characteristics owing to its easy way of analyzing complicated geometries. In this study, all the simulations are based on PVDF substrate, employed with commercially available finite element analysis, COMSOL Multiphysics 6.0 package, including two physics of solid mechanics and electrostatics following the piezoelectric equations, as shown in equations (1) and (2). Among other FEM tools, the COMSOL model is more reliable by including the piezoelectric effect and its dependence on the external impact, such as strain on a real scale with exact material properties. The essential properties to be specified for piezoelectric materials are compliance matrix [s], electrical permittivity [ε], and density [ρ]. Additionally, poling direction plays a vital role in the piezoelectric material in COMSOL, which is set to the z-axis in default.

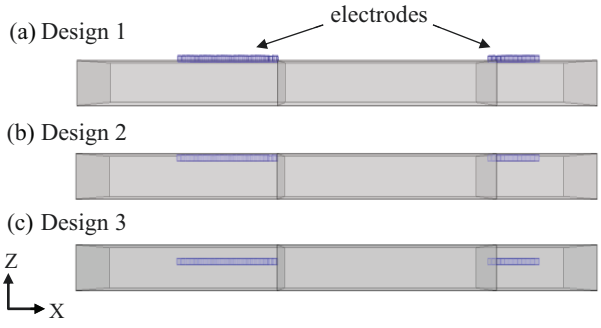

Figure 1: Different sensor configuration (a) Design 1, IDTs on surface, (b) Design 2, IDTs embedded immediate to surface, and (3) Design 3, IDTs embedded three times the thickness below surface

A 3D model with three different positions of electrodes along the thickness direction, as shown in Figure 1, is studied in both time and frequency domains. The boundary conditions used during the simulation include a fixed constraint on the bottom surface and low-reflective boundary conditions at the side walls to avoid border reflections. For the IDTs, an electrode pattern made of gold with 200μm wavelength maintaining a 50% metallization ratio, λ/4 width of 50 μm and thickness of 50 μm with 850 μm aperture, is designed and placed in different places along the thickness direction (design 1: on the surface, design 2: embedded immediately below the surface and design 3: three times the thickness of electrode below the surface). Overall, the model with IDTs and substrate is meshed using a tetrahedral element with a size of λ/8 and λ/4, respectively.

Table 1: Material properties used in numerical simulation

Description	Value
Polyvinylidene fluoride (PVDF)	
Density ρ [kg/m^3]	1780
Young's modulus E [GPa]	3
Poisson's ratio ν	0.3
Elastic compliance matrix [10^{-10} Pa^{-1}]	s_{11} = 3.781 s_{12} = -1.482 s_{13} = -1.724 s_{33} = 10.92 s_{44} = 14.28 s_{66} = 11.1
Permittivity matrix	ε_{11} = 7.4 ε_{22} = 9.3 ε_{33} = 7.6
Electromechanical coupling factor k^2	0.14
Gold (Au)	
Density ρ [kg/m^3]	19300
Young's modulus E [GPa]	70
Poisson's ratio ν	0.44

Table 1 lists the required material properties assigned to the substrate and electrodes from the COMSOL library. The numerical simulation studies are executed at two levels – time and frequency domain analysis.

2.1.1 Frequency-domain study

A frequency-domain analysis is studied to calculate the scattering parameter [S_{21}], which displays how much signal exists within a specific band at a given range of frequencies. The terminal feature is used in COMSOL to evaluate the frequency-based S-parameter. The terminated type connects the aimed terminal to a characteristics impedance that represents the wave transmission from input to output IDTs. Input power of 0.01 W is given to the sensor based on the power used in VNA for the experimental measurement, whose input power is 10 dBm. The S-parameter is measured in terms of insertion loss (IL), representing the power loss that occurs when the signal travels

through the transmission system. The obtained frequency peak information shown in Figure 2 for different designs is mentioned in Table 2.

Table 2: Center frequency peak information

Configuration	Center frequency [MHz]	Insertion loss [dB]
Design 1	3.81	116
Design 2	3.85	125
Design 3	4.00	137

An increase in insertion loss is observed with each design's distinct frequency peak information respective to the wave characteristics. Embedding the electrode completely below the substrate still exhibits an evident resonant peak that can be utilized as a sensor with acoustic wave propagation. This frequency study will stand out as a reference point for further analysis to dictate the performance of the sensor before fabrication.

(a) Design 1

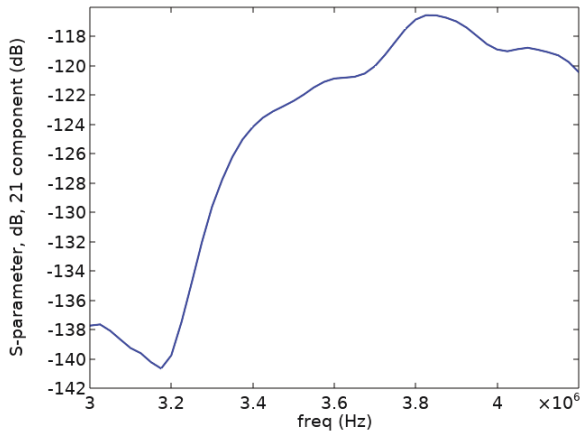

(b) Design 2

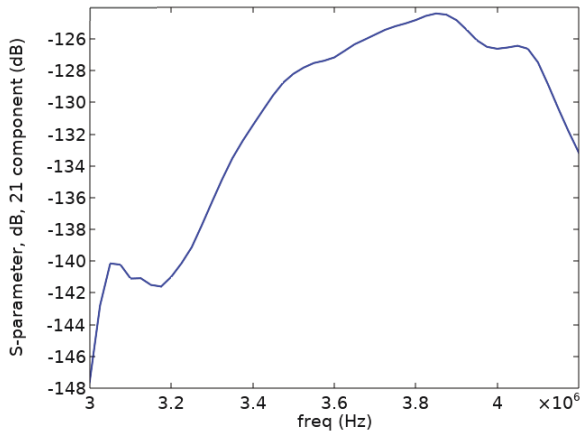

(c) Design 3

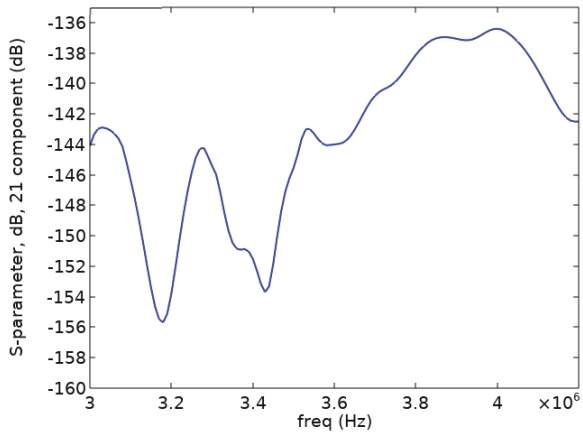

Figure 2: Frequency domain S_{21} response (a) Design 1, (b) Design 2, and (c) Design 3

2.1.2 Time-domain study

A time-domain analysis is studied to evaluate the change in input signal over time. Transient analysis of PVDF based sensor model, with an input sinusoidal signal of 3.8 MHz and magnitude of 1V lasting 18 cycles (~4.75μs), is executed. This signal is applied to positive electrodes in the input IDT where the negative side is grounded. While running the transient analysis with a short pulse excitation, different wave modes that are generated will be separated after traveling a certain distance due to their velocity difference. Due to a large number of wave reflections between the electrodes, a slight fluctuation in the wave is noticed. Positive electrodes in the output IDT receives the mechanical wave and transforms it into a voltage response.

Table 3: Time-domain analysis information

Configuration	Time delay [μs]	Output signal amplitude [mV]
Design 1	3.16	0.43
Design 2	3.42	0.18
Design 3	3.63	0.04

It is also noticed that the width of the received wavelength shows consistency with the wavelength of the input signal. The obtained time delay and amplitude of received voltage response information for different designs are shown in Figure 3, and values are mentioned in Table 3. It is noticed by embedding the electrodes, the amplitude level decreases with an increase in time to reach the output IDTs, as the substrate material surrounds it.

The time delay information is collected at a specific wave mode's amplitude, in which velocity is decreased by embedding the electrodes below the surface.

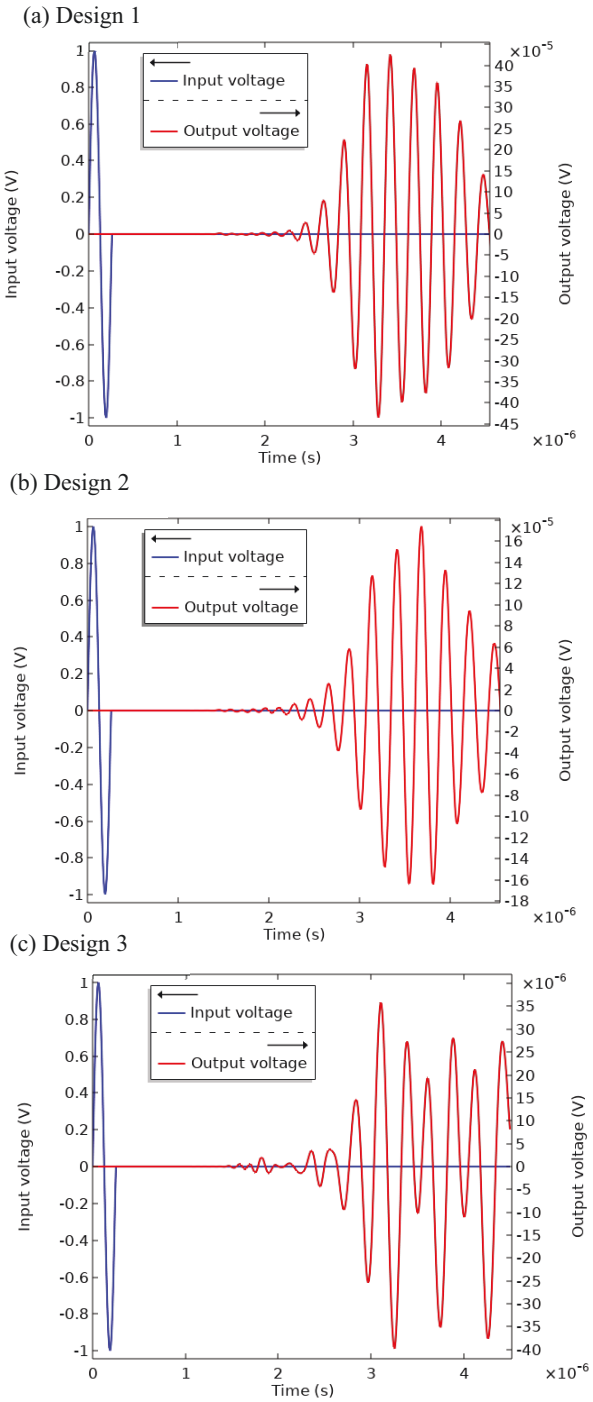

Figure 3: Time-domain voltage response (a) Design 1, (b) Design 2, and (c) Design 3

2.2 Theoretical modeling

The coupling of modes (COM) model is a widely accepted theoretical model, among other models such as impulse response, green's function model, and equivalent circuit model [13-16] due to its advantages such as the inclusion of second-order perturbation effects, which makes this model more reliable and accurate to the realistic case. The COM model uses a set of first-order wave equations, propagating in forward and backward modes with an electrical port. The waves are described by r (x, ω) and s (x, ω), representing modes propagating in the positive and negative x-direction.

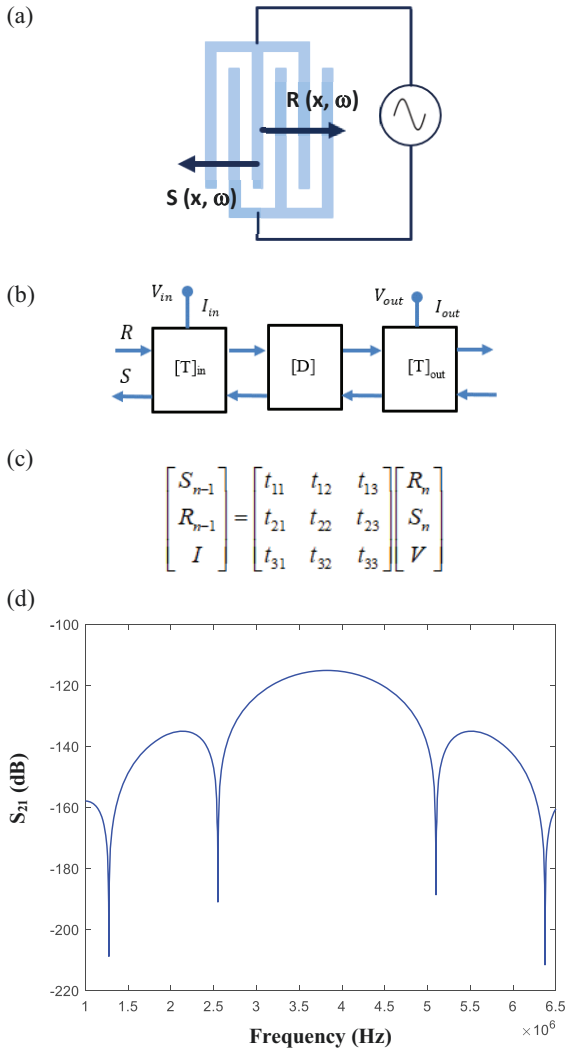

Figure 4: (a) Schematic of bi-directional IDTs with forward and backward waves, (b) transmission line of a three-component sensor device, (c) modified transmission matrix, and (d) center frequency response of design 1 using COM model

These two waves are initially uncoupled and unperturbed before the presence of grating, whose wave equations in the time domain are described as follows,

$$\frac{dR\ (x,\omega)}{dx} = -jk_R(x,\omega)R(x,\omega) \tag{3}$$

$$\frac{dS\ (x,\omega)}{dx} = +jk_R(x,\omega)S(x,\omega) \tag{4}$$

$$k_R = \frac{2\pi}{\lambda_R} = \frac{\omega}{\vartheta_R(x,\omega)} \tag{5}$$

where $\vartheta_R(x,\omega)$ denotes the spatially and frequency-dependent velocity of the Rayleigh wave. The wave propagating through the electrode gratings is frequency-dependent and the first-order wave equation in the frequency domain is derived using the Fourier transform.

A modified transmission matrix based on the COM model is utilized to increase the computational speed of the model, with a major component of metalized, non-metalized, and delay line regions, as shown in Figure 4 (a, b, and c). Material properties and IDT dimensions, such as thickness, aperture, number of input, and output finger pairs (same values used in the numerical approach), are given as inputs to the model. The theoretical response with a center frequency of about 3.79 MHz, as shown in Figure 4 (d), is obtained with 115 dB insertion loss, which shows an agreement with the center frequency obtained from the numerical model for design 1. Additionally, the numerical model is suitable only for design 1 with surface waves.

2.3 Strain analysis

For the strain analysis, initial strain conditions are applied from no strain to 10,000 με with 2,500 με increments. The strain and ambient phenomena are accounted as the static load, while the input signal is a harmonic load. The root mean squared (RMS) displacement is used to replace the S_{21} parameter based on the numerical tool used. Strain is applied in the longitudinal direction, and from the obtained response, as shown in Figure 5, there is an evident frequency shift with an increase in applied strain, which fits the fact that external strain leads to additional loss of signal power.

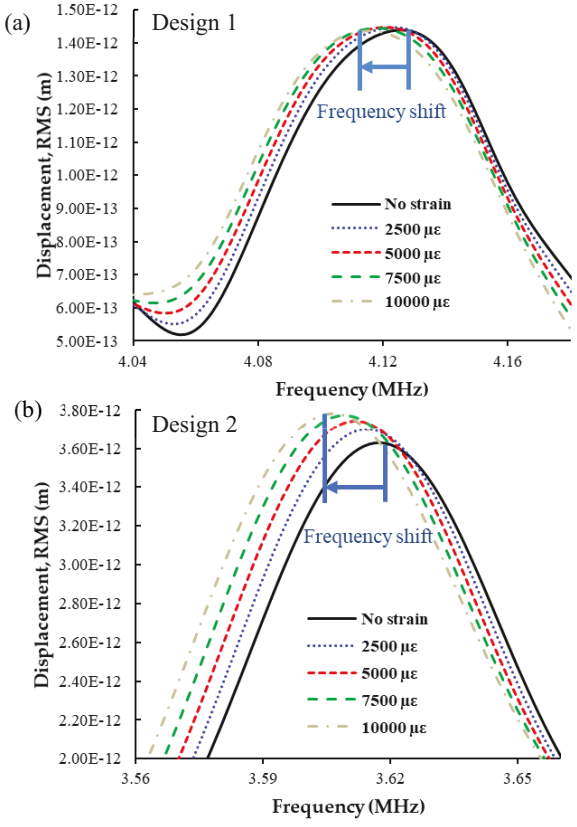

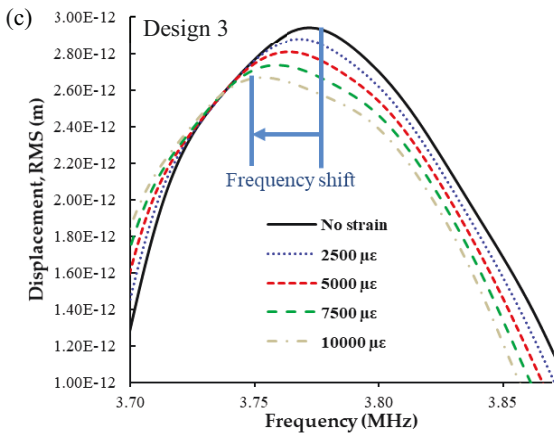

Figure 5: Numerical Strain analysis showing a shift in frequency peak (a) Design 1, (b) Design 2, and (c) Design 3

This change in frequency shifts occurs due to the combination of changes in IDT geometry and acoustic wave velocity, particularly with different designs used in this study. The numerically obtained shift in frequency with corresponding strain values is utilized to plot each design's sensitivity, as shown in Figure 6. Comparing different designs, embedding the electrode below the surface shows an increase in sensitivity associated with wave velocity and frequency response. A maximum sensitivity of 0.47 ppm/με is obtained in design 3, which significantly supports the embedding concept in this study.

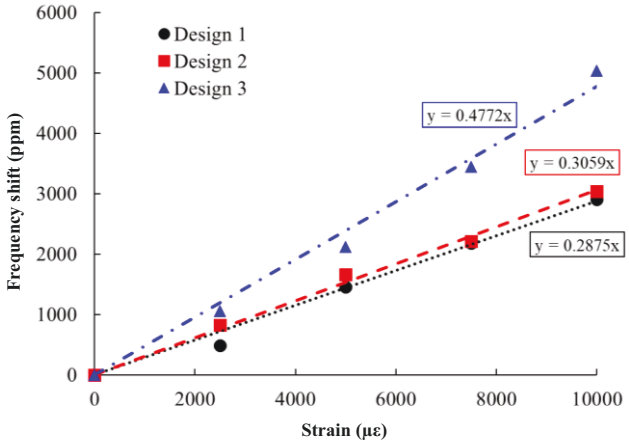

Figure 6: Resonance frequency shift vs strain values for wave-based sensor

3. EXPERIMENTAL WORK

3.1 Sensor development

A PVDF transparent film (PolyK Technologies, PA, USA, P056) is used as a piezoelectric substrate to deposit electrodes for experimental validation. The PVDF substrate's material properties, such as piezoelectric strain coefficient (d_{33}) of 23 pC/N and young's modulus of 1.2 GPa, are measured using a piezometer (YE2730A) and a universal testing machine AMETEK CS225 (Berwyn, PA, USA). For electrode deposition, a stencil made of negative photoresist (IP-Q) with an IDT pattern

is designed using the exact dimensions used in the numerical model and developed using a two-photon polymerization based GT2 printer (Photonic Professional GT2, Nanoscribe GmBH Karlsruhe, Germany) equipped with a 780 nm femtosecond laser and a 0.3 numerical aperature (NA) lens.

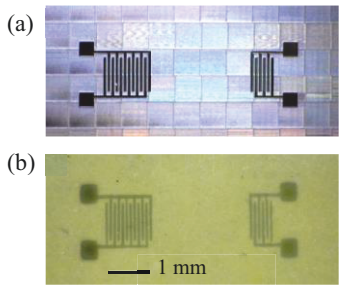

Figure 7: (a) 2PP printed stencil and (b) Gold sputtered electrodes

The printer parameters used to print the stencil are 4 µm slicing distance, 1 µm hatching distance, 100 mm/scan, and 90% laser power on a 2" silicon wafer. The stencil is removed using a sharp razor blade after heating on a hot plate at 100°C for 10 seconds. The gold sputtering technique is used to deposit the electrode on the substrate with the stencil placed on top, which acts as a mask where the electrode material is transferred onto the PVDF substrate, except in areas made impermeable to the gold by a blocking mesh. Figure 7 (a) and (b) show the 2PP printed stencil and electrode pattern through the gold sputtering technique without discontinuity.

3.2 Strain detection validation

Digital image correlation (DIC), an optical strain measurement technique, is performed to show quantitative displacement that occurred in Y-direction. The area under the sensor, as shown in Figure 7, especially the region under the IDT and delay line, is selected as a region of interest. Figure 8 shows the averaged strain concentration values under a designated area with different bent angles.

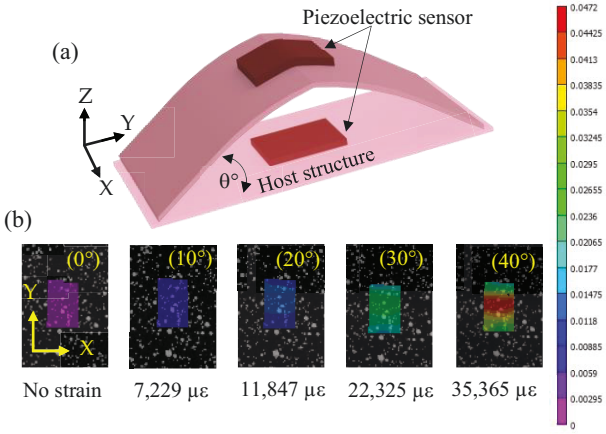

Figure 8: (a) VNA and DIC test setup with piezoelectric sensor attached to the host structure bent at angle θ° and (b) Digital image correlation of displacement in Y direction with average strain measured in selected area

The electro-acoustic frequency response behavior of the sensor (design 1) is studied using a Keysight N5227B vector network analyzer and two (ECP 18-GSG-1250-DP) probes. The sensor response at flat and different bent angles, as shown in Figure 8 (a), is measured in a frequency range from 44 MHz to 54 MHz, where the resonance peak provides information about the strain that occurred in the host structure. An evident shift in frequency peak is obtained, as shown in Figure 9, which validates the strain detection capability of the developed sensor. Due to the cabling effect and impedance mismatch, the center frequency peak is not detected, which needs to be investigated further along with sensitivity analysis.

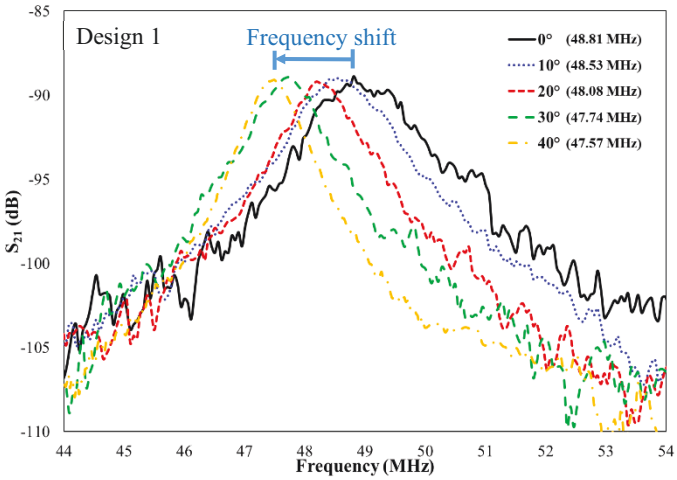

Figure 9: Scattering parameter response of piezoelectric sensor showing the frequency shifts at different angles

4. CONCLUSION

This paper presents the numerical, theoretical model, and fabrication procedure of acoustic wave-based piezoelectric sensor based on PVDF polymer substrate and gold electrodes. The change in wave characteristics of the sensor with different electrode configurations is studied in both time and frequency domains and is validated using a COM theoretical model. Among different designs, the embedded electrode concept (design 3) shows a higher sensitivity of 0.47 ppm/µε to the applied mechanical strains, despite the degradation in signal amplitude. Experimental measurements of developed sensor (design 1) show a correlation between the frequency response and quantitative mechanical strain. By establishing a detailed numerical study on embedded electrodes, this paper will stand out as a reference for future fabrication of sensors made of embedded electrodes through an advanced 2PP process with higher sensitivity towards intended application.

ACKNOWLEDGEMENTS

This material is based upon work supported in part by the National Science Foundation under Grant No. 2018853.

REFERENCES

[1] Ji, Z.; Zhang, M. Highly sensitive and stretchable piezoelectric strain sensor enabled wearable devices for real-time monitoring of respiratory and heartbeat simultaneously. *Nanotechnology and Precision Engineering* **2022**, *5*, 013002.

[2] Mandal, D.; Banerjee, S. Surface Acoustic Wave (SAW) Sensors: Physics, Materials, and Applications. *Sensors* **2022**, *22*, 820.

[3] Srinivasaraghavan Govindarajan, R.; Xu, X.; Sikulskyi, S.; Madiyar, F.; Rojas-Nastrucci, E.; Kim, D. Additive manufacturing of flexible nanocomposite SAW sensor for strain detection. In Proceedings of Sensors and Smart Structures Technologies for Civil, Mechanical, and Aerospace Systems 2021; p. 115910F.

[4] Srinivasaraghavan Govindarajan, R.; Rojas-Nastrucci, E.; Kim, D. Surface Acoustic Wave-Based Flexible Piezocomposite Strain Sensor. *Crystals* **2021**, *11*, 1576.

[5] Sirohi, J.; Chopra, I. Fundamental understanding of piezoelectric strain sensors. *Journal of intelligent material systems and structures* **2000**, *11*, 246-257.

[6] Achour, B.; Aloui, N.; Fourati, N.; Zerrouki, C.; Yaakoubi, N. Modelling and simulation of SAW delay line sensors with COMSOL Multiphysics. In Proceedings of MOL2NET 2018, International Conference on Multidisciplinary Sciences, 4th edition; p. 5887.

[7] Bharati, M.; Rana, L.; Tomar, M.; Gupta, V. Theoretical simulations of SAW based sensor on PVDF. *Materials Today: Proceedings* **2021**, *47*, 1538-1541.

[8] Bing, C.Y.; Mohanan, A.A.; Saha, T.; Ramanan, R.N.; Parthiban, R.; Ramakrishnan, N. Microfabrication of surface acoustic wave device using UV LED photolithography technique. *Microelectronic engineering* **2014**, *122*, 9-12.

[9] Bunea, A.-I.; del Castillo Iniesta, N.; Droumpali, A.; Wetzel, A.E.; Engay, E.; Taboryski, R. Micro 3D Printing by Two-Photon Polymerization: Configurations and Parameters for the Nanoscribe System. In Proceedings of Micro; pp. 164-180.

[10] Srinivasaraghavan Govindarajan, R.; Stark, T.; Sikulskyi, S.; Madiyar, F.; Kim, D. *Piezoelectric strain sensor through reverse replication based on two-photon polymerization*; SPIE: 2022; Vol. 12046.

[11] Li, L.; Peng, B.; Zhu, J.; He, Z.; Yang, Y.; Zhang, W. Strain Measurements With Langasite SAW Resonators at High Temperature. *IEEE Sensors Journal* **2020**, *21*, 4688-4695.

[12] Zhang, Q.; Han, T.; Tang, G.; Chen, J.; Hashimoto, K.-y. SAW characteristics of AlN/SiO 2/3C-SiC layered structure with embedded electrodes. *IEEE Transactions on Ultrasonics, Ferroelectrics, and Frequency Control* **2016**, *63*, 1608-1612.

[13] Kuypers, J.H.; Pisano, A.P. Green's function analysis of Lamb wave resonators. In Proceedings of 2008 IEEE Ultrasonics Symposium; pp. 1548-1551.

[14] Srinivasaraghavan Govindarajan, R.; Rojas-Nastrucci, E.; Kim, D. Strain sensing using flexible surface acoustic wave sensor. In Proceedings of Sensors and Smart Structures Technologies for Civil, Mechanical, and Aerospace Systems 2020; p. 1137912.

[15] Wang, T.; Green, R.; Guldiken, R.; Wang, J.; Mohapatra, S.; Mohapatra, S.S. Finite element analysis for surface acoustic wave device characteristic properties and sensitivity. *Sensors* **2019**, *19*, 1749.

[16] Hao, W.; Liu, J.; Liu, M.; Liang, Y.; He, S. Mass sensitivity optimization of a surface acoustic wave sensor incorporating a resonator configuration. *Sensors* **2016**, *16*, 562.